Thermal strain measurement in sol-gel lead zirconate titanate thin films

T. A. Berfield,[1,a)] J. F. Carroll III,[2] D. A. Payne,[3] and N. R. Sottos[3]
[1]*Department of Mechanical Engineering, University of Louisville, Louisville, Kentucky 40292, USA*
[2]*Sandia National Laboratory, Albuquerque, New Mexico 87185-1411, USA*
[3]*Department of Materials Science and Engineering, University of Illinois at Urbana-Champaign, Urbana, Illinois 61801, USA*

(Received 15 July 2009; accepted 21 September 2009; published online 16 December 2009)

A fluorescence-based digital image correlation (DIC) technique is used to characterize the in-plane strain development of blanket sol-gel derived lead zirconate titanate thin films deposited on platinized silicon substrates. The in-plane strain is also measured within film line features patterned via a mediated octadecyltrichlorosilane (ODS) monolayer. The results indicate that the selective film failure induced by the mediated ODS layer succeeds in slightly reducing the in-plane strain transverse to the line feature direction (~25% lower), while remaining nearly the same as the blanket film case in the direction parallel to the line direction. Additional in-plane stress estimates from wafer curvature measurements for the two film configurations (blanket and ODS patterned) were consistent with the DIC measured strain results. © *2009 American Institute of Physics*.
[doi:10.1063/1.3251420]

I. INTRODUCTION

Sol-gel based solution deposition is a popular option for the rapid, repeatable fabrication of electroceramic thin films. For lead zirconate titanate (PZT), the sol-gel deposition route is particularly attractive as it can lower the required firing temperature from 1100–1200 °C to the 650–750 °C range.[1,2] In addition to cutting back on fabrication costs, a reduced firing temperature is important to the production of quality PZT thin films for performance reasons. Electroceramics are susceptible to thermal stresses arising from the mismatch between film and substrate expansion coefficients, as well as intrinsic stresses due to material transformations upon cooling from firing temperature. Lowered firing temperatures translate to reduced thermal stresses and, thus, a lesser likelihood of film failure.[3] The downside that the unique nature of the sol-gel film deposition methodology brings is that additional shrinkage and densification related stresses originate early in the thermal processing stages, which may also be significant.

Stress development in electroceramic films is of interest as several studies have linked higher levels of processing related stresses to diminished ferroelectric properties. The ferroelectric properties of electroceramic thin film systems are highly dependent on the degree of residual stress,[4] as well as on the development of stress during the thermal processing stages of film fabrication. Tuttle and co-workers[5,6] found that for solution deposited PZT thin films, the stress state during the firing process affected the microstructure by regulating the relative populations of *a* versus *c* domains. It was proposed that domains preferentially aligned either parallel (*c* or 180° domains) or perpendicular (*a* or 90° domains) to the substrate, depending on the magnitude and sign (tensile or compressive) of the in-plane stress as the film is cooled through the transition temperature.[5,6] Lee *et al.*[7] showed that a compressive stress applied to PZT thin films during the firing process improved the piezoelectric response, while Lappalainen *et al.*[8] found an improvement in the dielectric constant as the PZT film thickness increased and the estimated residual stress levels decreased.

Few studies have probed the evolution in mechanical response for sol-gel films throughout the drying and densification processes, or the effects of film patterning on the stress development. Scherer[9] established the key steps in the drying sol-gel process as a complicated interconnect between evaporation, deformation of the solid phase, and fluid flow through the gel network. For the PZT sol-gel in this study, the two primary solvents are water (bp of 100 °C) and 2-methoxyethanol (bp of 125 °C). Upon heating, the PZT sol-gel films undergo a complex process of shrinkage and densification. Initially, the gel network collapses as solvents are driven off (approximately 100–130 °C), followed by pyrolosis.[10] The thermal expansion coefficient mismatch between the film and the substrate also induces an in-plane strain within the film.

Existing measurement tools for strain measurement on thin films are limited to bulge test apparatuses,[11] tensile testing of underetched samples,[12] or nanoindentation.[13] None of these techniques is well suited to quantify the mechanical response of thin blanket sol-gel films under thermal loading. Moreover, patterned films add another layer of complexity to the measurement. The aim of this work is to offer an optical technique for measuring thermal strain development within sol-gel thin films based on digital image correlation (DIC) and report values of in-plane strain as a function of temperature for both blanket and patterned film features.

II. MATERIALS AND EXPERIMENTAL METHODS

A. Material system

Single-side polished Si (100) wafers with a nominal thickness of 375 μm were used as the substrate for thin film

a)Electronic mail: tom.berfield@louisville.edu.

deposition. Wafers with a diameter of 3 in. were purchased commercially from Silicon Quest, Inc., with a prefabricated 500 nm thick surface layer of the thermally grown oxide. The bare wafers were cleaned using nanopure de-ionized water, acetone, and isopropyl alcohol, followed by a 10 min UV box treatment to remove any surface organics.

A bottom electrode was applied to the substrates by sputter coating under an argon environment using an AJA International cosputtering system. The AJA sputter-coating system allowed for consecutive deposition of thin films of different materials, while the substrate remained under vacuum, minimizing contamination and oxidization of the surface between layers. A 30 nm adhesion layer of titanium (Ti) was deposited, followed immediately by a 170 nm thick layer of platinum (Pt).

The sol-gel solution prepared for the fabrication of Pb-based perovskite thin films was processed using a synthesis route initially developed by Budd *et al.*,[14] which was later refined by Lakeman *et al.*[15] The composition of PZT in this study was $Pb(Zr_{0.53}Ti_{0.47})O_3$. The partially hydrolyzed solution was synthesized at a molarity of 0.25 and a $0.5R_w$ molar ratio of water to alkoxide. The concentrations were selected such that the resulting solution viscosity was well suited for spin-coating deposition.

Blanket films were fabricated by depositing 1.0 ml of the solution through a 0.2 μm filter onto a substrate spinning at 3000 rpm. The resulting films had a uniform thickness of 39 ± 0.5 nm, as measured by ellipsometry. In addition to blanket film specimens, patterned films were fabricated as a periodic array of line features (1.3 mm in width, with 1.3 mm spacing). A process that involved selectively inking the platinized substrate with a mediated monolayer was used to facilitate patterning of film features.[16–18]

The first step in patterning film features was the fabrication of a photoresist mask on each platinized substrate using positive-tone photolithography. A 2.5 μm thick layer of AZ5214E photoresist (Clariant Corp.) was spin cast onto the platinized substrate (60 s at 2500 rpm) and then the specimen was placed on a hot plate at 110 °C for 60 s. Next, the film was placed in a MJB3 Mask Aligner (Suss Microtech). The transparency photomask was securely positioned above the sample and brought into contact mode. The sample was then exposed to UV light for 10 s at a rate of 13.3 mW/cm^2. The entire film was removed and placed in a beaker of AZ327MIF (Metal Ion Free) developer. After approximately 90 s of mild agitation, the soluble photoresist is completely dissolved and the patterned features were clearly visible. The sample was removed from the developing agent and rinsed thoroughly with de-ionized water in a sonication bath. The resulting photoresist line feature is shown in Fig. 1.

A monolayer was deposited over the photoresist features and exposed substrate. The monolayer was transferred via a blank polydimethylsiloxane (PDMS) stamp. The PDMS stamp was prepared for monolayer transfer by functionalizing the surface with a UV box treatment. A 10 mM solution of octadecyltrichlorosilane (ODS) in hexane was prepared and stirred for 10 min prior to deposition. The blank PDMS stamp was spin coated with the ODS solution at 2000 rpm for 60 s and then dried under a stream of nitrogen for 30 s.

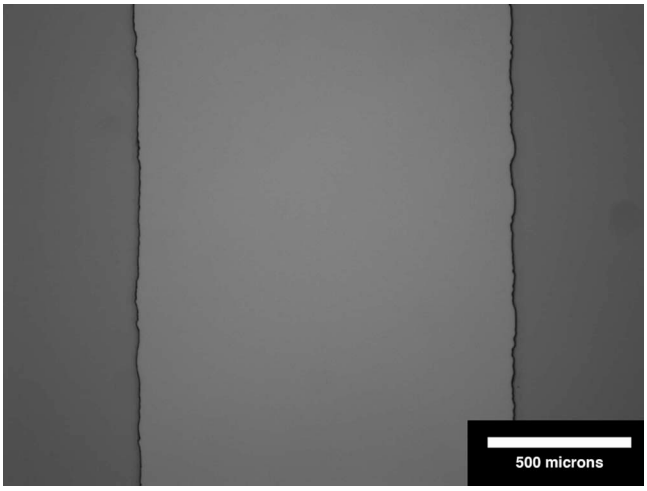

FIG. 1. Photoresist line feature (center) approximately 2.5 μm thick patterned by positive-tone photolithography on a $Pt/Ti/SiO_2/Si$ substrate.

The ODS covered stamp was brought into contact with the substrate for 1 min, transferring an ODS monolayer to the exposed substrate surfaces.

The substrate was rinsed once with nanopure de-ionized water to promote a dense monolayer and to remove excess ODS. The substrate was then rinsed repeatedly (more the three times) with acetone to dissolve the photoresist features, followed by a sonication bath to remove any remaining photoresist. After drying under nitrogen, the regions covered by the ODS monolayer were nearly undistinguishable from the uncoated areas of the substrate. The monolayer patterned substrate was then immediately spin coated with the PZT sol-gel solution using the same conditions (60 s at 3000 rpm) as the blanket films.

The resulting film thickness on the ODS patterned substrates was identical to the blanket films directly deposited onto the platinized substrate, as confirmed by ellipsometry measurements. While blanket sol-gel films contained no distinguishing surface features, the sol-gel film in the mediated specimens appeared slightly darker in areas where the ODS monolayer was present [Fig. 2(a)]. Upon application of a mild heat treatment, widespread cracking of the sol-gel film occurs in the areas of the mediated ODS monolayer. In contrast, the sol-gel film directly on the platinized substrate remains intact, effectively patterning features such as the line shown in Fig. 2(b). A sonication bath and mild polishing were performed to remove the cracked film, leaving only the patterned sol-gel features.

B. Thermal strain measurement via DIC

Using a fluorescence-based DIC technique,[19,20] the thermal strain for blanket PZT sol-gel films was measured and compared to the strain response within film features created by mediated monolayer patterning. DIC is a data analysis method that applies a mathematical correlation algorithm to obtain kinematic information from digital images acquired during deformation.[21–23] For conventional two-dimensional DIC, samples are prepared for testing by the application of a random speckle pattern to their surface. Comparison of successive images reveals a deformed speckle pattern relative to

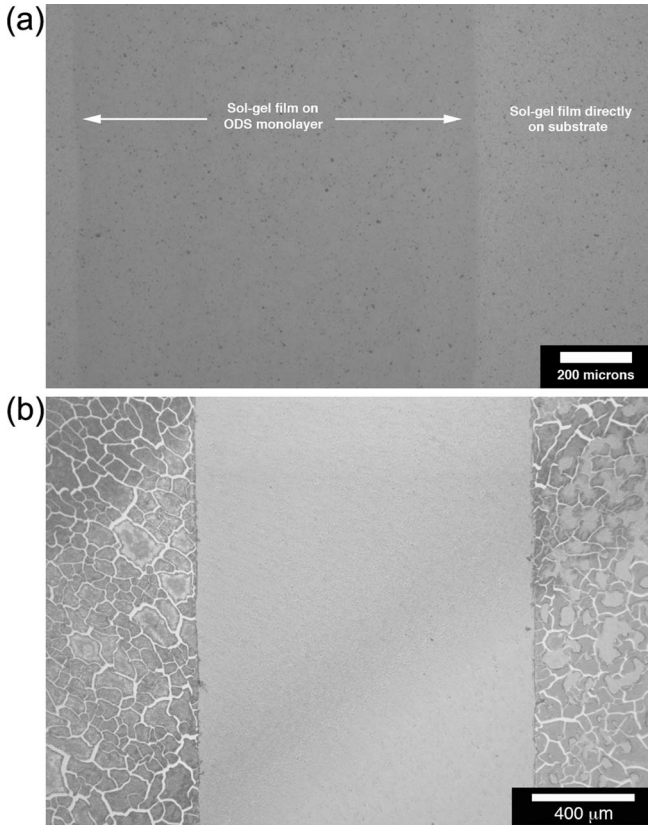

FIG. 2. Sol-gel film deposited onto an ODS monolayer patterned substrate (a) immediately after film deposition and (b) after thermal induced film failure (film selectively cracks in regions containing the ODS monolayer).

the initial, undeformed specimen surface. The correlation works by matching small square subsets of the undeformed image to locations in the deformed image. The core of the DIC method lies in the optimization of a correlation coefficient between the two subsets over six parameters characterizing the in-plane deformation; namely, the displacements components, u and v (in the x and y directions, respectively), and the displacement gradients, $\partial u/\partial x$, $\partial u/\partial y$, $\partial v/\partial x$, and $\partial v/\partial y$.[23] The accuracy of the method is approximately ± 0.1 pixel in displacement.

The DIC method requires that a suitable random speckle is present on the sample surface, and that images of the speckled surface are taken throughout the deformation process. Afterward, an algorithm is performed that breaks an image of the deformed surface into smaller subsets and correlates the subsets with the initial image of the undeformed surface. For this work, a least-squares fit based in-house algorithm developed at the University of Illinois by Abanto-Bueno and Lambros[24] was used. The rigid body motions (u and v), as well as the principal $(\partial u/\partial x, \partial v/\partial y)$ and cross $(\partial u/\partial y, \partial v/\partial x)$ derivative terms, are calculated directly.

However, PZT sol-gel thin films do not have a natural speckle pattern on the film surface. The films are featureless and lack any visible contrast on the surface across the size scale (approximately 200×200 μm^2) desirable for DIC measurements. The standard technique to create a random speckle pattern is to airbrush the surface with a black ink. Even with very fine nozzle airbrushing, though, ink droplets have a diameter (~ 10 μm) several times greater than the

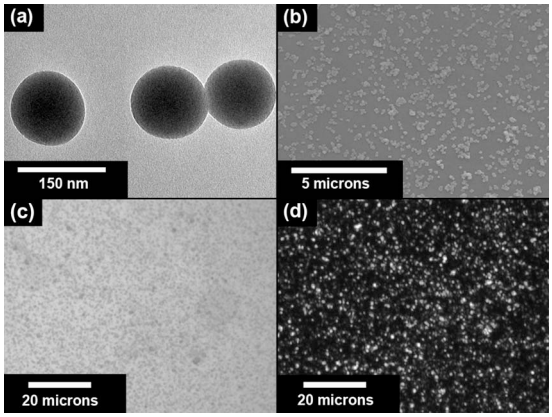

FIG. 3. (a) TEM image of silica labeled with a fluorescent core. (b) Scanning electron microscope image of a sol-gel film surface spin coated with the nanoparticles. (c) A nanoparticle coated sol-gel film imaged optically under white light and (d) fluorescent ($\lambda = 555$ nm) excitation.

thickness of the PZT sol-gel films used in this study. Additionally, achieving the proper dispersion of airbrushed ink droplets is often problematic.

Instead of ink, a suspension of fluorescent silica nanoparticles was used to create a suitable speckle pattern on the sol-gel film surface.[19,20] Fluorescent silica nanoparticles were fabricated using a recipe outlined by Van Blaanderen and co-workers.[25,26] The nanoparticles were made with a rhodamine fluorescent dye (maximum excitation wavelength of $\lambda = 555$ nm) incorporated at the core. Based on transmission electron microscope (TEM) images, the rhodamine labeled core of the silica particles was ~ 90 nm in diameter and, after the addition of a silica-only shell, the final diameter was ~ 140 nm [Fig. 3(a)]. The nanoparticles were then transferred to a dilute suspension (3% by mass) in ethanol and sonicated to ensure dispersion. When spin coated on the sample surface and excited, the fluorescent nanoparticles produced a speckle pattern ideal for DIC measurements that could be imaged optically, as shown in Fig. 3(d).

The system used to image the specimens was a Leica DMR microscope with a $0.63\times$ relay lens, $50\times$ long working distance objective, and a Q-Imaging Retiga monochrome digital camera (1.3 Mpixel). These imaging components produced a pixel resolution of 213 nm/pixel and a displacement resolution of 1/6 of a pixel. A complete baseline and displacement resolution tests using this imaging system were performed previously.[19,20]

Samples were placed under fluorescent excitation and heated at a rate of 10 °C/min up to 300 °C using a LinkAm THMS 600 thermal stage. Throughout the heating process, images were taken with the optical microscope system. Using the in-house DIC code,[24] images were correlated with the initial room temperature image. Strains were directly computed for subsets of 41×41 pixels and were averaged over a 650×650 square pixel area.

C. In-plane stress estimates via wafer curvature

In addition to the DIC in-plane strain analysis, wafer curvature measurements were performed separately to estimate the development of in-plane stress. Both blanket films

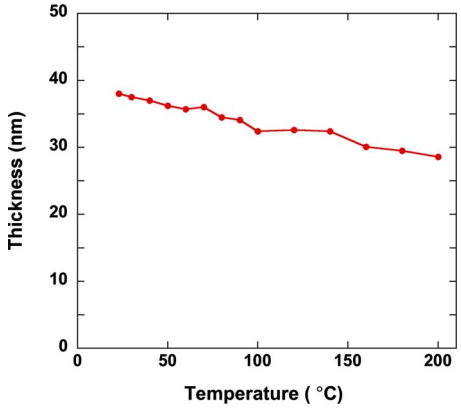

FIG. 4. (Color online) Ellipsometry measurements (λ=633 nm) to determine the thickness of a single layer sol-gel film deposited (0.25 M at 3000 rpm for 60 s) on a $Pt/Ti/SiO_2/Si$ substrate as it is heated at a rate of 10 °C/min.

and ODS patterned line features were deposited onto full 3 in. substrates as described above. Films were then placed in a FLX-2908 laser reflectance system, which measured the wafer curvature along a single axis within a thermal chamber. The temperature was ramped at 10 °C/min up to 180 °C, with curvature measurements taken approximately every 5 °C.

From the changes in the wafer curvature, the Stoney equation was used to find the stress in a blanket thin film during the course of thermal loading. The average biaxial stress (σ) in a blanket thin film is given by the Stoney equation as[27]

$$\sigma = \left(\frac{E_s}{1-\nu_s}\right)\frac{t_s^2}{6t_f}\left(\frac{1}{R}-\frac{1}{R_0}\right). \quad (1)$$

From Eq. (1), the stress in the film is found as a function of the change observed in the radius of curvature (R) from the baseline curvature (R_0) and the substrate elastic properties, Young's modulus (E_s), and Poisson's ratio (ν_s). The equation is a result of force and moment balance between the film and the substrate. Although the substrate thickness (t_s) is constant, the film thickness (t_f) does change with temperature.

To account for film thickness changes associated with solvent removal, film thickness was monitored by ellipsometry while under the identical thermal cycle. A single layer sol-gel film was placed on a thermal stage under a Gaertner L116C single wavelength (λ=633 nm) ellipsometer and heated at a rate of 10 °C/min up to 180 °C. Over this temperature range, the film thickness decreased by 25% (Fig. 4).

For the patterned line features, the regularity of line features allows for the computation of the in-plane stress using wafer curvature measurements along both principal axes and a modified Stoney equation. Given a periodic array of identical line features, Yeo *et al.*[28] presented a relation between the in-plane stress and the curvature change ($\Delta 1/R$) in the directions transverse ($\perp$) and parallel ($\parallel$) to the line features. The in-plane stresses along the axes perpendicular and parallel to the line direction are, respectively,[28]

$$\sigma_\perp = \frac{E_s t_s^2}{6(1-\nu_s^2)t_f(\mathrm{AC})}\left(\Delta\frac{1}{R_\perp}+\nu_s\Delta\frac{1}{R_\parallel}\right). \quad (2)$$

$$\sigma_\parallel = \frac{E_s t_s^2}{6(1-\nu_s^2)t_f(\mathrm{AC})}\left(\Delta\frac{1}{R_\parallel}+\nu_s\Delta\frac{1}{R_\perp}\right). \quad (3)$$

In Eqs. (2) and (3), the terms for material properties and thickness are consistent with those used in the Stoney equation (1). The change in curvature in each principal direction ($\Delta 1/R_\parallel$ and $\Delta 1/R_\perp$) is with respect to a baseline, unstressed reference curvature. The AC term is the area coverage that refers to the relative area of the substrate covered by the film material. The assumption is made here that no stress is held by the regions in which film cracking occurs. For the periodic array of lines used in this study, the area coverage was 0.50 as the linewidth and spacing are equal.

To calculate the average stress for the line features via the modified Stoney equations (2) and (3), the change in the radius of curvature in both principal directions (parallel and perpendicular to the line direction) was required. However, the KLA-Tencor FLX-2908 laser reflectance system could only measure the wafer curvature along one direction during heating. Due to this limitation, the stress for sol-gel line features was estimated by measuring the wafer curvature change along each separate principal axis for multiple samples fabricated in same fashion. The in-plane stress at a given temperature was estimated by using the radius of curvature change parallel to the line features from one sample and the curvature change perpendicular to the lines from a second sample tested under the identical conditions. This test was repeated multiple times to verify the validity of this approach.

III. RESULTS

A. DIC results

As expected, heating caused a biaxial tensile state within the blanket sol-gel films. The measured ε_{xx} and ε_{yy} strains were nearly identical and increased linearly with temperature. For all films tested, a small spike in the strain was repeatedly observed at 150 °C and was likely due to film pyrolysis or interactions with the Pt bottom electrode. The subset displacement vector data and the radial displacement contours for the blanket film response at temperatures of 80, 140, 220, and 300 °C are shown in Fig. 5. Across the region of interest, the sol-gel film expanded symmetrically in both principal directions.

The patterned film specimens experienced a different strain evolution than the blanket films. For the mediated films, sol-gel deposited on ODS regions consistently began cracking between 60 and 70 °C. From 70 to 150 °C, cracking spread throughout the mediated ODS regions until only distinct islands existed. Beyond 150 °C, the islands underwent shrinkage. The line features between the mediated regions showed no readily observable changes (cracking, etc.) throughout the entire heating range. DIC measurements on the line film features showed an asymmetric strain response. In-plane strains for the ε_{xx} direction (perpendicular to the line direction) and the ε_{yy} direction (parallel to the line) were

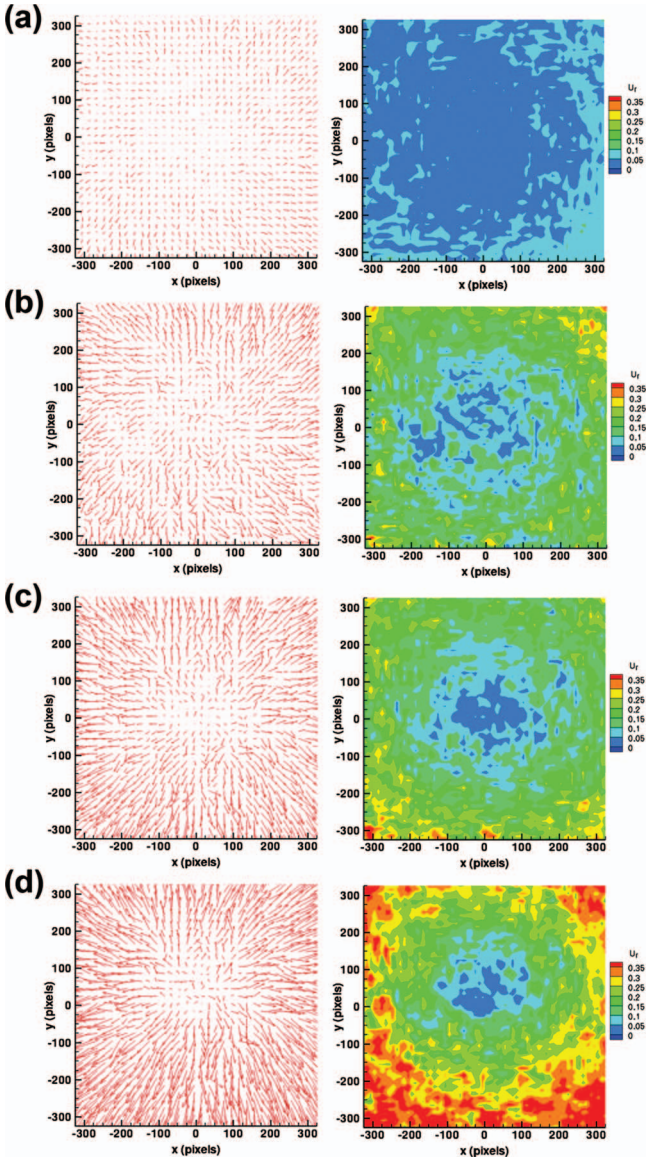

FIG. 5. (Color) DIC results of the thermal test of a blanket single layer sol-gel film, showing the vector and radial displacement contours at (a) 80 °C, (b) 140 °C, (c) 220 °C, and (d) 300 °C. The resolution is 213 nm/pixel.

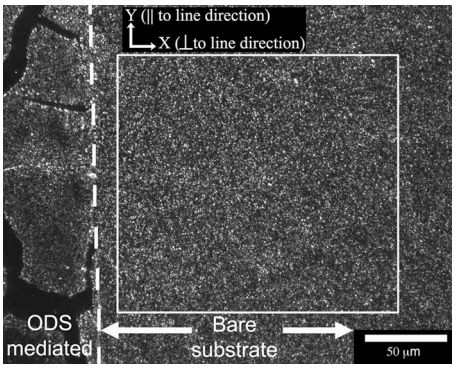

FIG. 6. Image of cracked sol-gel film patterned into a line feature via a mediated ODS monolayer at high magnification under fluorescent excitation. The boxed region represents the area over which DIC is performed and where the average in-plane strains are calculated.

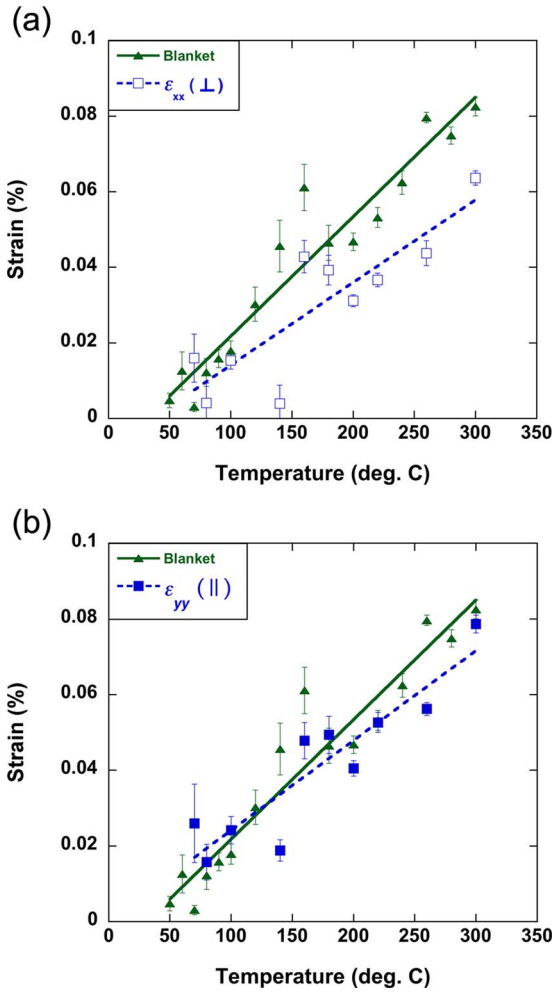

FIG. 7. (Color online) The blanket film strain is compared to the strain for an ODS patterned line feature in (a) the ε_{xx}, or transverse direction, and (b) in the ε_{yy}, or parallel direction. Both films are initially 39 nm thick and heated at 10 °C/min. Data are shown with a linear best fit.

calculated over subsets in the region of the line feature, as shown in Fig. 6(a), and averaged. The standard deviation for each average strain value reported is represented by error bars (Fig. 7).

The ε_{xx} component of the strain in the line feature is compared to the ε_{xx} strain for the blanket film case in Fig. 7(a). After the onset of cracking of the mediated film regions, the tensile strain that developed perpendicular to the line direction was consistently lower for the patterned line feature than for the blanket case at the same temperature. However, the ε_{yy} strain component for the line feature (parallel to the line direction) [Fig. 7(b)] was always higher than that in the perpendicular direction. The slope of the best fit line for the ε_{yy} strain component of the line feature was slightly lower than that for the blanket film case.

The difference in the measured tensile strain between the blanket films and for both the line and island features in the ε_{xx} direction increased with the temperature. At the highest temperature tested, 300 °C, the blanket film experienced a strain of 0.082%. At the same temperature, the strain measured in the ε_{xx} direction was 0.064% for the line case. In the ε_{yy} direction, the strain for the line feature was 0.079%, which was much closer to the blanket case.

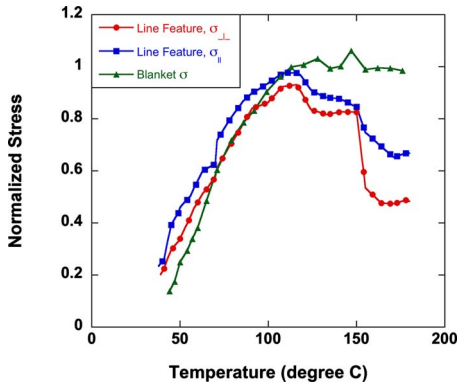

FIG. 8. (Color online) In-plane stress calculated for a blanket single layer sol-gel film compared to the stress in an ODS patterned line feature both perpendicular and parallel to the line direction. Stresses are normalized by the stress for the blanket film at 180 °C (218 MPa).

B. Stress measurement results

The results of thermally induced stress for the single layer blanket sol-gel films and the ODS patterned line features under heating are compared in Fig. 8. The results are normalized by the stress for the blanket film at 180 °C (218 MPa) to illustrate the qualitative differences between the two samples. Although cracking in the film regions with mediated ODS monolayer consistently initiated between 60 and 70 °C, no significant deviation in the stress was observed between the samples until 115 °C. For the blanket case, the sol-gel film was highly constrained by the substrate, causing shrinkage and densification to primarily occur in the thickness direction. In the line feature case, film failure released constraint in the direction perpendicular to the line, allowing some in-plane movement and tensile stress relief within the feature. The biaxial tensile stress for the blanket case leveled off at higher temperatures while the stress in the line features began to drop. At the maximum temperature, the estimated stress in the line feature perpendicular to the line direction was approximately 50% that of the blanket case. Parallel to the line direction, the estimated stress in the line feature was 68% of the blanket case. Heating beyond 180 °C causes a material transformation within the sol-gel film, making stress measurement more complex.

IV. DISCUSSION AND CONCLUSIONS

In situ thermal strains were measured for blanket films as a function of temperature using DIC. Combined with a thorough study of the microstructural and chemical evolution of sol-gel derived PZT thin films during thermal processing, these strain measurements provide insight into the strain development throughout the complex film densification process. This method has potential to probe the effects of solvent substitution, or other material system variations, on the stress-strain development within sol-gel films.

The in-plane tensile strains that develop within the ODS patterned features are lower than those for the blanket case. Hence, mediated monolayer patterning offers a method for controlling and relieving the development of tensile strain within PZT thin films, which, in turn, may correspond to improved ferroelectric properties. Strain measurements obtained by fluorescence-based DIC reveal that patterning introduces substantial variations in the mechanical state of thin film features even in large feature sizes. For features with higher aspect ratios, the changes in the stress-strain state are expected to be more pronounced. These results verify that assumptions of ferroelectric performance for patterned film features based on studies of blanket films need to adjust for deviations in the stress state introduced by the particular patterning method.

Stress estimates based on the wafer curvature measurements are in agreement with the results of the DIC analysis. The stress in the direction parallel to the ODS patterned line features is very close to that measured for the blanket case, as both configurations have nearly the same degree of constraint. In contrast, the stress in the transverse direction of the patterned films is much lower than that for the parallel direction.

The stresses that developed during the solvent evaporation phase of thin film processing represent only a portion of the cumulative final residual stress state. The mediated monolayer patterning did not alter other factors that contribute to the stress, such as the intrinsic transformation stress or the thermal expansion mismatch. However, these results do reveal that mediated monolayer patterning of film features alters the stress during the early stages of development.

The in-plane strain development within PZT sol-gel thin films subjected to thermal loading was measured using a fluorescence-based DIC method. Mediated patterning significantly reduces in-plane strain development within patterned features but is highly dependent on the feature geometry. Additionally, in-plane stress estimates based on wafer curvature measurements provided consistent evidence of reduced stress levels in mediated monolayer patterned features.

ACKNOWLEDGMENTS

The authors would like to acknowledge the Lambros Research Group in the Aerospace Engineering Department at the University of Illinois for providing the DIC code used in this work. In addition, the Braun Research Group in the Materials Science and Engineering Department is acknowledged for assistance in silica nanoparticle fabrication. The authors would also like to acknowledge and thank the National Science Foundation for funding this research through Grant Nos. 88206 and CMMI 07-26742. Some of this work was based on previous studies that were supported by the U.S. Department of Energy, Division of Materials Sciences, under Award No. DEFG02-91ER45439 through the Frederick Seitz Materials Research Laboratory at the University of Illinois at Urbana-Champaign.

[1]M. Klee, R. Eusemann, W. Brand, and H. van Hal, J. Appl. Phys. **72**, 1566 (1992).
[2]Z. Huang, Q. Zhang, and R. W. Whatmore, J. Appl. Phys. **85**, 7355 (1999).
[3]M.-H. Zhao, R. Fu, D. Lu, and T.-Y. Zhang, Acta Mater. **50**, 4241 (2002).
[4]T. A. Berfield, R. J. Ong, D. A. Payne, and N. R. Sottos, J. Appl. Phys. **101**, 024102 (2007).
[5]B. A. Tuttle, J. A. Voight, T. J. Garino, D. C. Goodnow, R. W. Schwartz, D. L. Lamppa, T. J. Headley, and M. O. Eatough, Proceedings of the Eighth IEEE International Symposium on Applications of Ferroelectrics, 1992 (unpublished), p. 344.

[6]B. A. Tuttle, T. J. Garino, J. A. Voight, T. J. Headley, D. Dimos, and M. O. Eatough, Proceeding of NATO Advanced Research Workshop on Science and Technology of Electroceramic Thin Films, 1995 (unpublished), p. 117.
[7]J.-W. Lee, S.-M. Lee, C.-S. Park, G.-T. Park, and H.-E. Kim, J. Sol-Gel Sci. Technol. **42**, 305 (2007).
[8]J. Lappalainen, J. Franti, and V. Lantto, J. Appl. Phys. **82**, 3469 (1997).
[9]G. Scherer, J. Non-Cryst. Solids **87**, 199 (1986).
[10]C. D. E. Lakeman, Z. Xu, and D. A. Payne, J. Mater. Res. **10**, 2042 (1995).
[11]Y. Xiang, X. Chen, and J. J. Vlassak, J. Mater. Res. **20**, 2360 (2005).
[12]Y.-W. Cheng, D. T. Read, J. D. McColskey, and J. E. Wright, Thin Solid Films **484**, 426 (2005).
[13]M. Zhao, Y. Xiang, J. Xu, N. Ogasawara, N. Chiba, and X. Chen, Thin Solid Films **516**, 7571 (2008).
[14]K. D. Budd, S. K. Dey, and D. A. Payne, Br. Ceram. Proc. **36**, 107 (1985).
[15]C. D. E. Lakeman and D. A. Payne, J. Am. Ceram. Soc. **75**, 3091 (1992).
[16]N. L. Jeon, P. Clem, D. Y. Jung, W. Lin, G. S. Girolami, D. A. Payne, and R. G. Nuzzo, Adv. Mater. (Weinheim, Ger.) **9**, 891 (1997).
[17]D. A. Payne and P. G. Clem, J. Electroceram. **3**, 163 (1999).
[18]E. A. Mikalsen and D. A. Payne, Solid State Ionics **151**, 53 (2002).
[19]T. A. Berfield, J. K. Patel, R. G. Shimmin, P. V. Braun, J. Lambros, and N. R. Sottos, Small **2**, 631 (2006).
[20]T. A. Berfield, J. K. Patel, R. G. Shimmin, P. V. Braun, J. Lambros, and N. R. Sottos, Exp. Mech. **47**, 51 (2007).
[21]W. H. Peters and W. F. Ranson, Opt. Eng. (Bellingham) **21**, 427 (1982).
[22]W. H. Peters, W. F. Ranson, M. A. Sutton, T. C. Chu, and J. Anderson, Opt. Eng. (Bellingham) **22**, 738 (1983).
[23]H. A. Bruck, S. R. McNeill, M. A. Sutton, and W. H. Peters, Exp. Mech. **29**, 261 (1989).
[24]J. L. Abanto-Bueno and J. Lambros, Exp. Mech. **45**, 144 (2005).
[25]A. van Blaaderen and A. Vrij, Langmuir **8**, 2921 (1992).
[26]N. A. M. Verhaegh and A. van Blaaderen, Langmuir **10**, 1427 (1994).
[27]G. G. Stoney, Proc. R. Soc. London, Ser. A **82**, 172 (1909).
[28]I.-S. Yeo, P. S. Ho, and S. G. H. Anderson, J. Appl. Phys. **78**, 945 (1995).